PCCP

ROYAL SOCIETY OF CHEMISTRY

PAPER

View Article Online
View Journal | View Issue

Cite this: *Phys. Chem. Chem. Phys.*, 2025, **27**, 8949

Unveiling the synthesis mechanisms of (Bi,Sb,Sn)–Te and observation of the n-type to p-type semiconducting transition in Sb–Bi_2Te_3 nanostructured chalcogenides derived *via* an aqueous-based reflux method†

V. R. Akshay*[abc] and M. Vasundhara*[abd]

Received 6th June 2024,
Accepted 17th March 2025

DOI: 10.1039/d4cp02312a

rsc.li/pccp

A systematic study of a surfactant-assisted, aqueous-based, low-temperature chemical method for the synthesis of (Bi,Sb,Sn)–Te nanostructures was carried out. A detailed understanding of the chemistry involved in the reaction mechanism and decomposition of ethylenediaminetetraacetic acid was proposed for different precursors of Bi, Sb and Sn, and the possibilities for the aqueous-based, low-temperature synthesis of phase pure Bi_2Te_3, SnTe, and Sb_2Te_3 was demonstrated. The reaction mechanism revealed that the aqueous-based reflux reaction is suitable for the synthesis of Bi_2Te_3, unsuitable for the synthesis of SnTe, and suitable for the partial formation of Sb_2Te_3. Hot-pressed Sb-doped Bi_2Te_3 samples exhibited an n- to p-type semiconducting transition with variations in temperature and Sb dopant concentration. A significant improvement in Seebeck coefficient and power factor values of 215.12 μV K^{-1} and 7.1 μW m^{-1} K^{-2}, respectively, was observed at 465 K for the 5% Sb-doped Bi_2Te_3 nanostructures. This work focuses primarily on the reaction mechanism of Bi-, Sb- and Sn-based tellurides in an aqueous medium, providing further possibilities in the field of chalcogenide nanostructures for thermoelectric applications.

1. Introduction

Increased energy demand since the last decade has boosted the interest in highly efficient materials for power generation and cooling applications. Thermoelectric (TE) materials are a class of materials that can reversibly convert heat energy into electrical energy. By analyzing the TE principles, the TE performance of materials can be efficiently optimized. A material with a high TE performance should have a good electrical conductivity (σ), high Seebeck coefficient (S) for electronic transport, appropriate carrier concentration and low thermal conductivity (κ) for maintaining the temperature difference. Tuning the carrier concentration and κ through various methods is an efficient way to adjust the TE properties of materials. A dimensionless quantity called the figure of merit (ZT) is a measure of the TE efficiency of any material, which is generally expressed using the following relation:[1]

$$ZT = S^2\sigma\frac{T}{\kappa} = \frac{S^2T}{\rho(\kappa_L + \kappa_e)}$$

Specifically, the focus is on high-performance TE devices comprising n- and p-type components derived from high ZT materials. A series connection is maintained electrically and a parallel connection is maintained thermally on these TE devices or modules. From the above relation, it is clear that a good TE material should possess a "phonon-glass electron-crystal" (PGEC) behavior, resulting in a large S.[2] Interestingly, the researchers aim to win the conflict among the interdependent parameters S, σ and κ, and generally, it is an extremely tedious job to satisfy these criteria in any TE material possessing simple crystal structures. With these conflicting properties, any attempt to improve any of the S, σ or κ parameters may significantly deteriorate other properties and thereby the overall TE performance. By considering this key issue, it is interesting to observe that there is a possibility of getting a prominently increased value of power factor ($S^2\sigma$) when the carrier concentration is nearly 10^{19}, which is exhibited by the materials in the region where there is a crossover among metals and semiconductors.[2]

[a] *Materials Science and Technology Division, CSIR-National Institute for Interdisciplinary Science and Technology, Thiruvananthapuram-695019, India. E-mail: mvas@iict.res.in, vasu.mutta@gmail.com, vijayrajakshay@gmail.com*
[b] *Academy of Scientific and Innovative Research (AcSIR), Ghaziabad-201002, India*
[c] *Mandelbrot Systems Pvt. Ltd, Thiruvananthapuram-695032, Kerala, India*
[d] *Polymers and Functional Materials Department, CSIR-Indian Institute of Chemical Technology, Uppal Road, Tarnaka, Hyderabad-500007, Telangana, India*

† Electronic supplementary information (ESI) available. See DOI: https://doi.org/10.1039/d4cp02312a

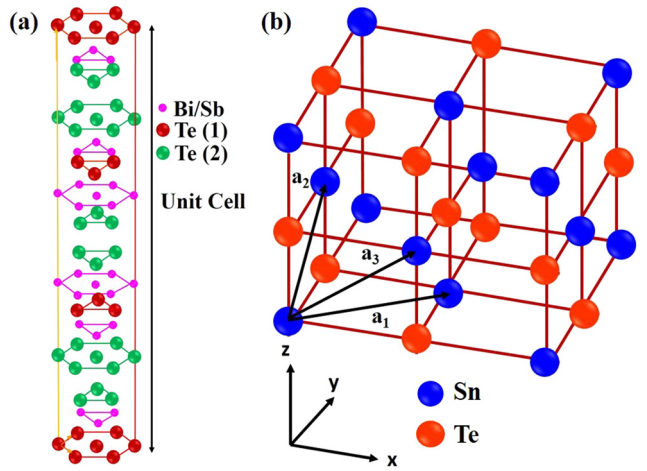

Fig. 1 Crystal structure of (a) Bi_2Te_3/Sb_2Te_3 and (b) SnTe.

The most studied and interesting TE materials in the chalcogenide category are Bi_2Te_3, Sb_2Te_3 and SnTe, which have a wide temperature range for thermoelectric applications. Reports on the aqueous-based synthesis of chalcogenide nanostructures are limited.[1,2] Due to the inherent transport properties, a hexagonal crystal structure is preferred for the thermoelectric applications of Bi_2Te_3 and Sb_2Te_3.[1]

Bi_2Te_3 and Sb_2Te_3 are narrow band gap semiconductors with homologous layered crystal structures having a rhombohedral unit cell with an $R\bar{3}m$ space group, possessing good σ and low κ and are used for power generation and in cooling devices.[3–5] Fig. 1(a) shows the layered crystal structure of M_2Te_3 (M = Bi and Sb) and is described by a hexagonal unit cell, as shown in Fig. 1. The unit cell is composed of five covalently bonded monatomic sheets along the *c*-axis in the sequence –Te(1)–Bi–Te(2)–Bi–Te(1)–Te(1)–Bi–Te(2)–Bi–Te(1)–. Bi_2Te_3 is reported to be an n-type semiconductor, while Sb_2Te_3 is a p-type semiconductor. However, the presence of excess Te may change their type from n-type to p-type semiconductors. Sb_2Te_3 and its doped derivatives have been widely studied due to their excellent *ZT* in the temperature range of 300–500 K.[6–8] The self-generation of anti-site defects creates a large number of holes in bulk Sb_2Te_3 owing to a low *S*.[6] As a consequence, the *ZT* values are limited to about 1 over the entire temperature range, which corresponds to low efficiencies of the TE device, limiting wider applications. Venkatasubramaniam *et al.*[9] proposed a specially constructed Bi_2Te_3/Sb_2Te_3 superlattice with a *ZT* of 2.4 at room temperature. Recently, Yang *et al.*[10] synthesized Sb_2Te_3 nanostructures and achieved a *ZT* of 0.37 at 473 K by employing a surfactant-assisted reflux method and utilizing cold compaction, followed by annealing. Several chemical methods have been employed to prepare nanostructures with different shapes. However, a single phase of Sb_2Te_3 could not be easily achieved due to the spontaneous occupation of partial Sb atoms at the Te lattice sites.[11] Wang *et al.*[12] synthesized hexagonal nanoplates of Sb_2Te_3 using a solvothermal approach. However, they showed a low *ZT* due to the Te impurity, which reduced the σ of the Sb_2Te_3 matrix. Hence, the majority of research work has been focused on the preparation of nanostructures with various techniques, while studies on the consolidation of Bi_2Te_3, Sb_2Te_3 and $Bi_{2-x}Sb_xTe_3$ nanocrystals and their thermoelectric properties are relatively rare.

SnTe is another narrow band gap semiconductor with a direct band gap of 0.18 eV. SnTe normally forms a p-type semiconductor due to Sn vacancies, and at low temperatures, it becomes a superconductor. SnTe exhibits a very low *ZT* ~0.40 at 900 K[13] due to its intrinsically high carrier concentration, large $\Delta E_{L\text{-}\Sigma}$ of 0.3 eV and high lattice thermal conductivity.[14,15] SnTe exists in 3 crystallographic phases. At low temperatures, where the hole concentration is less than 1.5×10^{20} cm^{-3}, SnTe exists in a rhombohedral structure and is known as α-SnTe. At room temperature and atmospheric pressure, SnTe crystallizes in the rock salt structure[16] and SnTe is composed of a face-centered cubic lattice of Te atoms with Sn atoms filling all the octahedral voids and is known as β-SnTe. The β-SnTe transforms to γ-SnTe at 18 kbar pressure, with an orthorhombic structure and Pnma space group. The β-SnTe (referred to as SnTe) with cubic structure and $Fm\bar{3}m$ space group finds application as TE materials. The crystal structure of SnTe is shown in Fig. 1(b).

SnTe has received limited attention as a TE material due to its inability to control its very high carrier concentration, which is of the order of 10^{21} cm^{-3} at 300 K, resulting in a low *S* and high κ_e.[17] A large concentration of intrinsic Sn vacancies is responsible for the high p-type carrier concentration in SnTe.[18] In SnTe, the energy difference between the light hole valence band (L band) and the heavy hole valence band (Σ band) is 0.3 eV.[17,19–23] The large energy separation between the light and heavy hole valence bands restricts the contribution of heavy hole mass to the Seebeck coefficient. Recently, alloying SnTe with other metal tellurides, such as $AgSbTe_2$, MgTe, SrSe, and CdSe, was found to improve its TE performance.[24–28] A remarkable enhancement in the *ZT* was achieved due to the formation of resonance levels in the valence band through In doping in SnTe synthesized by a high energy ball milling and spark plasma sintering.[29] Alloying of SnTe with SnSe, which has a high band gap of 0.9 eV, helps reduce the κ value and also results in an improved *S* due to the convergence of the two valence bands of SnTe. Moreover, the κ value of SnTe can be further decreased by the solid solution alloying with SnSe. Alloying Cd or Hg in SnTe also results in an enhancement in *S* due to the decreased energy separation between the light and heavy hole valence band.[30,31] In the present investigation, we have synthesized the desired crystal structures of different chalcogenide materials such as Bi_2Te_3, Sb_2Te_3 and SnTe nanostructures using an aqueous-based low-temperature reflux method and investigated the feasibility of phase formation in an aqueous medium. The aqueous-based reflux method using $NaBH_4$ could successfully lead to the complete reduction of Te without the formation of TeO_2, which is highly desirable for the formation of phase pure compounds. Hence, we attempted to synthesize different chalcogenide materials to achieve a good control over the morphology. Further, the TE properties of Sb-doped Bi_2Te_3 nanostructures are also studied in the present work.

2. Experimental section

The Bi_2Te_3, Sb_2Te_3 and SnTe nanostructures were prepared using $BiCl_3$ (99.9%, metals basis, supplied by Alfa Aesar), Sb powder (99.999%, metals basis, supplied by Alfa Aesar), $SbCl_3$ (99.997%, metals basis, supplied by Alfa Aesar), $SnCl_2$ (99.99%, metals basis, supplied by Sigma Aldrich) and Te powder (99.99%, metals basis, supplied by Alfa Aesar) as metal ion precursors and ethylenediaminetetraacetic acid (EDTA) as the surfactant. Deionised water was used as the reaction medium, sodium borohydride ($NaBH_4$) as the reducing agent and the reaction was carried out at the boiling point of the medium. The detailed synthesis procedure is reported in our earlier studies.[1] After being stirred for 10 min, the solution was refluxed, which constitutes the primary stage of the reaction, where $BiCl_3$, $SbCl_3$ and $SnCl_2$ could ionize into the corresponding metal ions and chloride ions. EDTA is essential to cap the bismuth ions and to control the morphology over different reaction times. The reaction was carried out using a 4.4 M $NaBH_4$ and reaction time of 24 h to get stable and phase pure nanostructures based on our previous studies. In order to get the nanostructured Bi_2Te_3, a pH of 10 was maintained during the synthesis (using NaOH). As soon as the reaction was completed, the synthesized products were collected, centrifuged, washed with acetone, ethanol, and deionized water several times, and then dried under a vacuum environment at 373 K for 6 h. The further removal of EDTA in all the samples was ensured by heat treating at temperatures of 473, 533 and 623 K, respectively, for 3 h under inert conditions with intermediate grinding. The samples are labelled as BT, ST-1, ST-2 and TT for Bi_2Te_3, Sb_2Te_3 (using Sb powder), Sb_2Te_3 (using $SbCl_3$) and SnTe, respectively. The 1%, 3% and 5% Sb-doped Bi_2Te_3 samples are labelled as BS1T, BS3T and BS5T, respectively. The hot pressing of BS1T, BS3T and BS5T samples was carried out at 723 K and 60 Mpa, which are labelled as BS1T-HP, BS3T-HP and BS3T-HP, respectively. Their structures and phase purities were studied by powder X-ray diffraction (XRD) at room temperature using PANalytical X'Pert Pro diffractometer using Cu-Kα radiation and an X-ray wavelength of 1.5406 Å with a step size of 0.0167°. The particle size, morphology and crystallinity are characterized by high-resolution transmission electron microscopy and HR-TEM (FEI Tecnai F20, operated at 200 kV). To investigate the electrical properties, including electrical resistivity ($\rho = 1/\sigma$), S and the corresponding thermoelectric power factor $S^2\sigma$, a rectangular block (dimensions 3 mm × 3 mm × 15 mm) was taken from the hot-pressed pellet and measured in the ZEM-3 (ULVAC-RIKO) system under helium atmosphere from room temperature to 573 K.

3. Results and discussion

3.1. Structural analysis of Bi_2Te_3, Sb_2Te_3 and SnTe samples

Fig. 2 shows the XRD patterns of all the studied samples. A phase pure Bi_2Te_3 is obtained for BT with a hexagonal crystal structure and without any impurity peaks of Bi or Te. The BT sample matches well with the Bi_2Te_3 hexagonal phase with ICSD No: 20289. The observed peaks for ST1 correspond to the

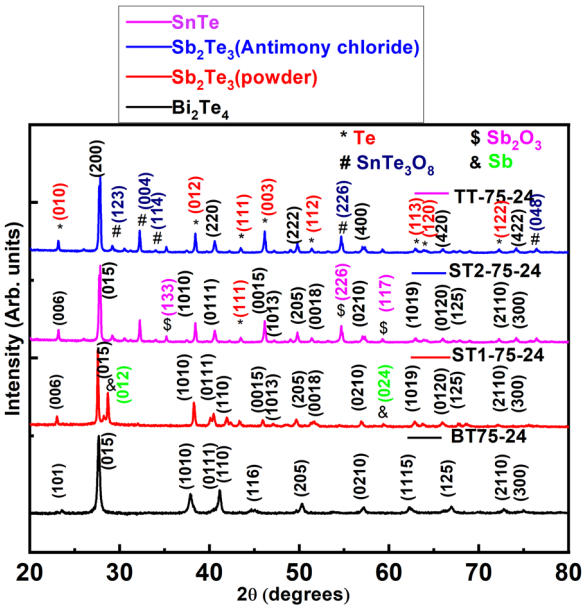

Fig. 2 XRD patterns of BT, ST1, ST2 and TT nanostructures.

diffraction from the hexagonal Sb_2Te_3 material having space group $R\bar{3}m$ with the JCPDS number 15-0874.[32] In addition, minor impurity peaks of Sb are noticed in ST1. It is observed that ST2 contains both Sb_2Te_3 peaks and several impurity peaks of intermediate phases such as Te and Sb_2O_3. A similar observation was also made for the TT sample, where impurity peaks such as $SnTe_3O_8$ and Te are present. Hence, the XRD results suggest that the formation of phase pure compounds of chalcogenides through an aqueous-based chemical method is feasible only for selected cases, especially for BT.

3.2. Mechanism of the thermal decomposition of EDTA

Ligands such as EDTA act as a capping agent for tailoring the crystal growth and may also provide the possibility of breaking the crystalline nature, which may lead to different morphologies and wider applications.[33–35] EDTA can coordinate with several inorganic ions to form multinuclear complexes. It is well-reported that such structures can also act as a template in the self-assembly process.[36–38] It is expected that an oriented attachment may occur with the template effect of EDTA by adding appropriate ligands to the reaction mixtures. Also, EDTA added as an anion surfactant in the solution could connect with Bi^{3+} ions to form large molecular groups, which facilitates Bi_2Te_3 nuclei to grow along the surfaces of EDTA agglomerates. When the EDTA selectively binds to one of the facets, the growth rate in either *a*- or *b*-axis directions kinetically slows down, with a relative increase in the *c*-axis direction. The movements of these fine hexagonal crystals together with molecular groups in the solution, make it possible for the particles to connect with each other by suspended bonds according to the definite epitaxy in the *c*-axis direction and consequently form long nanorods or nanosheets. These rods and sheets are arranged through the template action of the EDTA additive, which is a favourable mechanism as per the recent reports where expensive techniques such as solvothermal/hydrothermal methods and high reaction temperature were used to

develop the desired materials.[39–41] Hence, the EDTA-assisted synthesis using EDTA as a surfactant gives good control over the morphology and helps to prevent oxidation of the synthesized nanostructures.

However, EDTA residues in the final product can detrimentally affect its structural integrity, crystallinity and thermoelectric performance. To obtain the nanostructured Bi_2Te_3, a pH of 10 must be maintained during the synthesis (using NaOH) and finally, the precipitated product is to be washed with acetone, ethanol and deionized water several times. The residual EDTA can dissolve well in acetone when the pH is above 8; hence, from the slurry of the aqueous-based Bi_2Te_3 final product, EDTA and other unreacted residues can be removed by treating it initially with acetone till a clear solution is obtained. Again, upon heat treatment, the EDTA primarily decomposes to *N*-(2-hydroxyethyl) iminodiacetic acid and iminodiacetic acid at 473 K. At higher temperatures, *i.e.*, at 533 K, these primary products can yield ethylene glycol as the final product. Ethylene glycol controls the morphology of our nanostructures even at a sintering temperature of 623 K. Hence, EDTA is removed partially by washing with different solvents and partially by converting it to ethylene glycol at a higher temperature. The temperature-dependent decomposition of EDTA in the aqueous synthesis of chalcogenide nanostructures is explained as follows: At 533 K, EDTA decomposes into *N*-(2-hydroxyethy1)iminodiacetic acid and iminodiacetic acid, as shown in eqn (1). Further hydrolysis of *N*-(2-hydroxyethy1)iminodiacetic acid results in the formation of ethylene glycol and iminodiacetic acid (eqn (2)).[42]

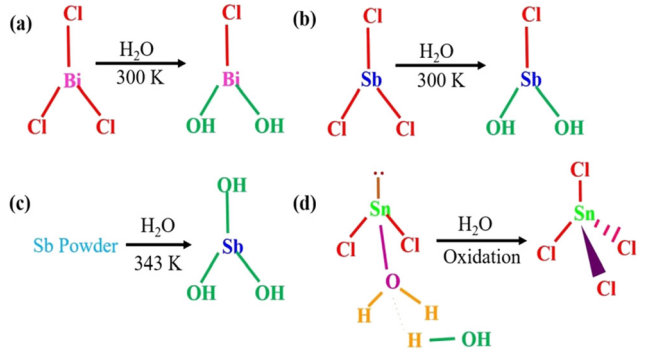

Fig. 3 Possible chemical compounds generating cations of (a) Bi, (b) and (c) Sb and (d) Sn to form the corresponding chalcogenide nanostructures.

Deng *et al.* synthesized Bi_2Te_3 nanorods using EDTA as the surfactant.[43] Srashti *et al.* synthesized Bi_2Te_3 nanostructures by a refluxing method using EDTA as a surfactant, KOH and $NaBH_4$ and showed that the growth and morphology of Bi_2Te_3 depends upon the surfactant, concentration of KOH and reaction timings.[44] Yang *et al.* showed that EDTA-Na_2 could be used as a complexing agent in the synthesis of nanocrystalline Sb_2Te_3 and achieved a power factor (PF) of 2.04 μW cm^{-1} K^2 at 140 °C and σ remained in the range of 5–10 × 10^3 S m^{-1}.[45] Dharmaiah *et al.* synthesized Sb_2Te_3 nanoplates using EDTA and achieved a high S of 181 μV K^{-1}, high σ of 763 Ω^{-1} cm^{-1} and low κ of 1.15 W m^{-1} K^{-1}.[46]

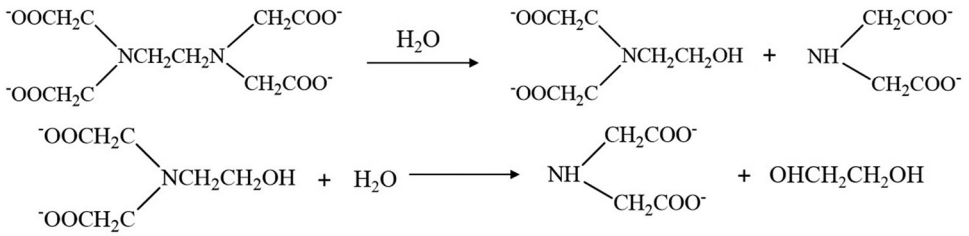

A portion of iminodiacetic acid decomposes to iminodiacetic anhydride with the evolution of water at 512 K (eqn (3)).

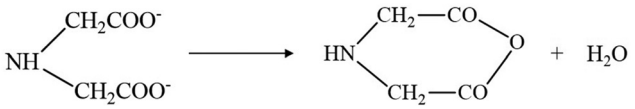

At around 593 K, iminodiacetic anhydride boils off. Beyond 593 K, iminodiacetic acid decomposes into water, carbon dioxide, carbon monoxide, acetonitrile and hydrogen gas as by-products, as shown in eqn (4). Acetonitrile boils at 354 K and ethylene glycol vaporises at 470 K.

3.3. Mechanism for the formation of secondary phases in Sb_2Te_3 and SnTe samples

To explore further the unstable phases of ST2 and TT, a detailed understanding of the chemistry of these materials is necessary. Let us consider the chemical reactions that could possibly occur in each case. Fig. 3 represents the chemical compounds that can generate Bi^{3+}, Sb^{3+} and Sn^{2+}/Sn^{4+} in an aqueous medium to combine with Te^{2-} to form the corresponding chalcogenide materials. The existence of Te^{2-} ions in the aqueous medium is validated with the chemical equations as represented in eqn (5)–(7).

$$3Te + 6OH^- \rightarrow 2Te^{2-} + TeO_3^{2-} + 3H_2O \quad (5)$$

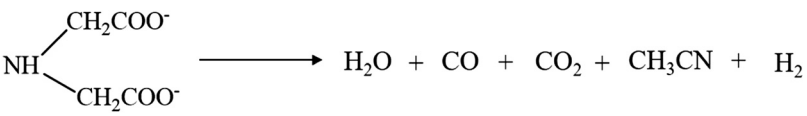

$$2TeO_3^{2-} + NaBH_4 \rightarrow Te^{2-} + Te + NaBO_3 + H_2O + 2OH^- \quad (6)$$

$$5Te + 10OH^- + NaBH_4 \rightarrow 5Te^{2-} + NaBO_3 + 7H_2O \quad (7)$$

While using $BiCl_3$ in the formation of Bi_2Te_3, it is obvious that $Bi(OH)_2Cl$, which is stable at room temperature, will generate Bi^{3+} ions in the aqueous medium, whereas $Bi_4O_5Cl_2$ and BiOCl will not take part in the chemical reaction,[47] as represented in eqn (8)–(12).[48]

$$4BiCl_3 + 5H_2O \xrightarrow{813\ K} Bi_4O_5Cl_2 + 10HCl \quad (8)$$

$$BiCl_3 + 2H_2O \xrightarrow{300\ K} Bi(OH)_2Cl + 2HCl \quad (9)$$

$$BiCl_3 + H_2O \xrightarrow{>400\ K} BiOCl + 2HCl \quad (10)$$

$$Bi^{3+} + [EDTA]^2 \rightarrow [Bi[EDTA]]^+ \quad (11)$$

$$3[Bi(EDTA)]^+ + 2Te^{2-} \rightarrow Bi_2Te_3 \quad (12)$$

Thus, the formation of stable BT nanostructures is possible using $BiCl_3$. While using $SbCl_3$ as the starting material, the following reactions could occur as mentioned below in eqn (13)–(17)

$$4SbCl_3 + 5H_2O \xrightarrow{323\ K} Sb_4O_5Cl_2 + 10HCl \quad (13)$$

$$SbCl_3 + 2H_2O \xrightarrow{300\ K} Sb(OH)_2Cl + 2HCl \quad (14)$$

$$SbCl_3 + H_2O \xrightarrow{343\ K} SbOCl + 2HCl \quad (15)$$

$$Sb^{3+} + [EDTA]^{2-} \rightarrow [Sb(EDTA)]^+ \quad (16)$$

$$3[Sb(EDTA)]^+ + 2Te^{2-} \rightarrow Sb_2Te_3 \quad \text{(partially)} \quad (17)$$

It is well understood from eqn (13) and (15) that the formation of $Sb_4O_5Cl_2$ and SbOCl is unavoidable, and only the partial synthesis of Sb_2Te_3 is possible. An easy way to obtain phase pure Sb_2Te_3 in an aqueous medium is through Sb metallic powder where $Sb(OH)_3$ can contribute Sb^{3+}, as shown in eqn (18).

$$Sb\ (\text{metallic powder}) + H_2O \xrightarrow{343\ K} Sb(OH)_3 + Sb^0 \quad (18)$$

A small trace of metallic Sb could be present here; still, this method is valid for eqn (16) and (17) to develop Sb_2Te_3 nanomaterials in an aqueous medium, which corroborates with the XRD results of ST1.

Interestingly, it is observed that the Sn-based reactions are not recommended in aqueous medium as Sn^{2+} can easily undergo oxidation to form Sn^{4+}, as represented in eqn (19)–(21).

$$SnCl_2 + H_2O \overset{323\ K}{\rightleftharpoons} Sn(OH)Cl + HCl \quad (19)$$

$$6SnCl_2(aq) + O_2(g) + 2H_2O \rightarrow 2SnCl_4(aq) + 4Sn(OH)Cl(s) \quad (20)$$

$$Sn^{2+} \xrightarrow[H_2O]{\text{oxidation}} Sn^{4+} \quad (21)$$

It could be seen that $SnCl_2$ reacts with water to form an insoluble basic salt Sn(OH)Cl. This basic salt could further combine with Te ions present in the solution to form a secondary phase $SbTe_3O_8$ in addition to SnTe. Thus, the aqueous-based synthesis using EDTA is not suitable for the synthesis of SnTe. Other methods, such as the one described in the recent report,[49] must be adopted to synthesize phase pure SnTe nanopowders.

In this regard, it could be presumed that there are limitations to the formation of Sb_2Te_3 and SnTe in aqueous-based reflux synthesis. However, the partial formation of Sb_2Te_3 using EDTA prompted us to synthesize Sb-doped Bi_2Te_3 and to investigate the n-to-p-type behaviour with Sb doping. Hence, we have attempted to synthesize Sb-doped Bi_2Te_3. Small amounts of Sb, such as 1%, 3% and 5%, were doped into the Bi site using the reflux method. The use of Sb powder may not bring satisfactory results, and hence, $SbCl_3$ was used as the precursor for the synthesis of Sb-doped Bi_2Te_3 as $SbCl_3$ will be suitable for replacing Bi ions to form the doped compound.

3.4. Structural analysis of Sb-doped Bi_2Te_3

Fig. 4 shows the XRD patterns of the Sb-doped BT samples prepared for 1%, 3% and 5% concentrations by keeping the molarity of $NaBH_4$ at 4.4 M. It could be seen that BS1T exists in a single phase at lower Sb concentrations and crystallizes into a hexagonal Bi_2Te_3 structure. However, BS3T and BS5T contain small amounts of secondary phases of Sb and Sb_2O_3. Hence, it could be seen that for higher concentrations of Sb, the samples do not become phase pure. Hence, the reflux method alone is not sufficient to produce phase-pure samples of Sb-doped Bi_2Te_3.

Hence, as a second step, these samples were hot pressed at a pressure of 50 MPa and a temperature of 723 K and the XRD patterns were obtained for the Sb-doped samples, as shown in Fig. 5(a). Upon hot pressing, all the Sb-doped BT samples crystallized into a combination of hexagonal Bi_2Te_3 and BiTe phases. The Rietveld refinement of all the samples is shown in Fig. 5(b)–(d). No

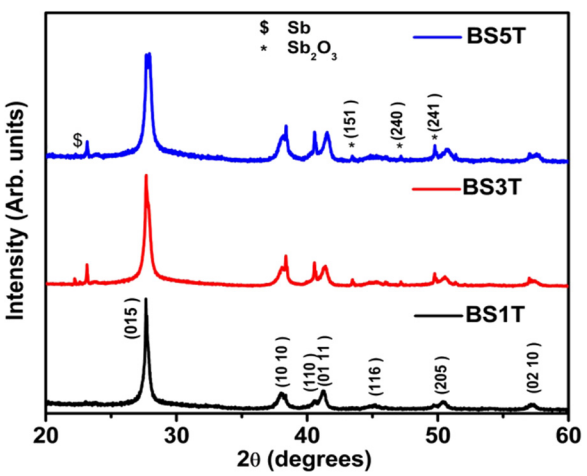

Fig. 4 XRD patterns of cold-pressed Sb-doped BT nanostructures.

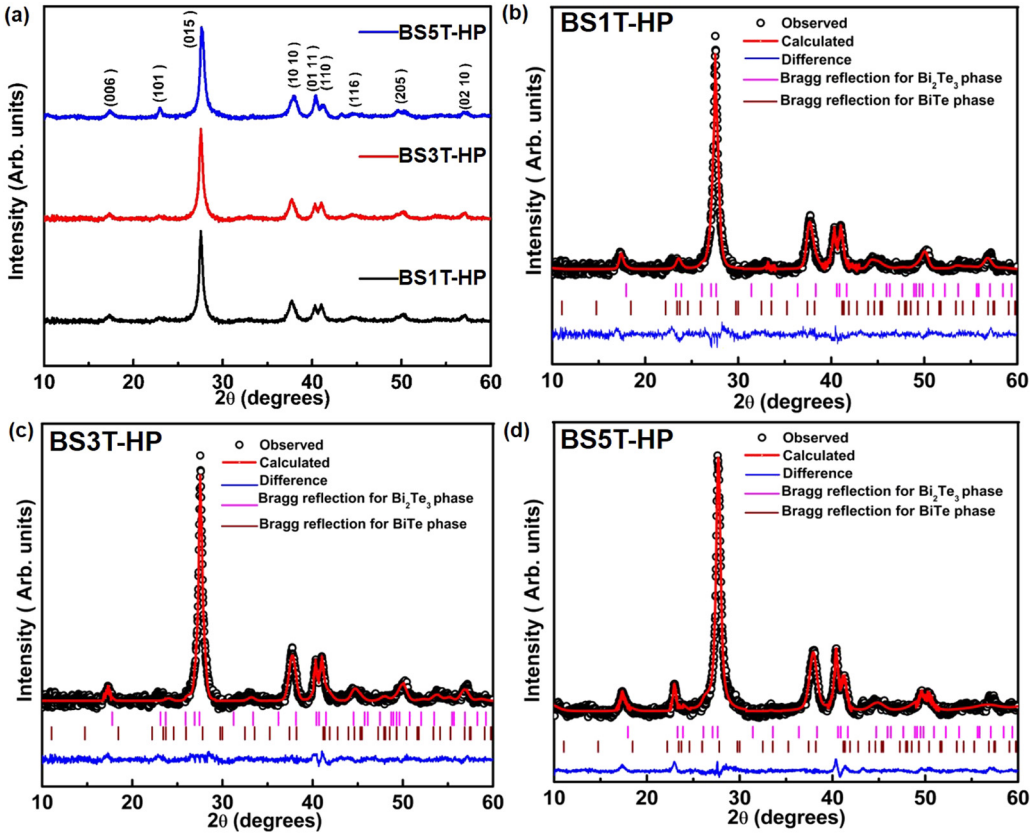

Fig. 5 (a) XRD patterns of hot-pressed Sb-doped BT nanostructures. Refined XRD patterns of (b) BS1T-HP, (c) BS3T-HP and (d) BS5T-HP.

peaks corresponding to Sb or Sb_2O_3 were indexed in the XRD patterns. The structural parameters determined from Rietveld refinement are listed in Table 1. A low value of χ^2 is observed, which justifies the quality and goodness of the refinement.

It is seen from the refinement data that there is a decrease in unit cell volume with an increase in Sb concentration. This is attributed to the small size of Sb^{3+} ions substituting Bi^{3+} ions in the lattice. Also, upon hot pressing, there could be a redistribution of ions in the lattice, and the insoluble compounds could have vaporised, leading to the formation of phase-pure Bi_2Te_3 without any impurity peaks.

3.5. Morphological analysis of hot-pressed Sb-doped Bi_2Te_3

Fig. 6(a) and (b) show the TEM images of BS1T-HP. The TEM images of BS1T-HP indicate the formation of nanosheets. The formation of nanosheets in BS1T-HP could be attributed to the template action of EDTA, as a result of which an oriented

Table 1 Refined XRD parameters of BS1T-HP, BS3T-HP and BS5T-HP

BTA structure	BS1T-HP		BS3T-HP		BS5T-HP	
Phase	Bi_2Te_3 + BiTe		Bi_2Te_3 + BiTe		Bi_2Te_3 + BiTe	
Crystal structure	Hexagonal + rhombohedral		Hexagonal + rhombohedral		Hexagonal + rhombohedral	
Space group	$R\bar{3}m$ + $P\bar{3}m1$		$R\bar{3}m$ + $P\bar{3}m1$		$R\bar{3}m$ + $P\bar{3}m1$	
Lattice parameters						
a (Å)	4.38(3)	4.34(8)	4.37(3)	4.34(8)	4.36(3)	4.35(8)
b (Å)	4.38(3)	4.34(8)	4.37(3)	4.34(8)	4.36(3)	4.35(8)
c (Å)	30.08(5)	24.80(9)	30.08(5)	24.80(9)	30.08(5)	24.80(9)
γ (deg)	120	120	120	120	120	120
Volume (Å)^3	504.99(6)	406.50(1)	504.99(6)	406.50(1)	504.99(6)	406.50(1)
Residual parameters						
R_p	3.40		3.34		3.27	
wR_p	2.29		2.13		2.09	
χ^2	1.89		1.68		1.54	

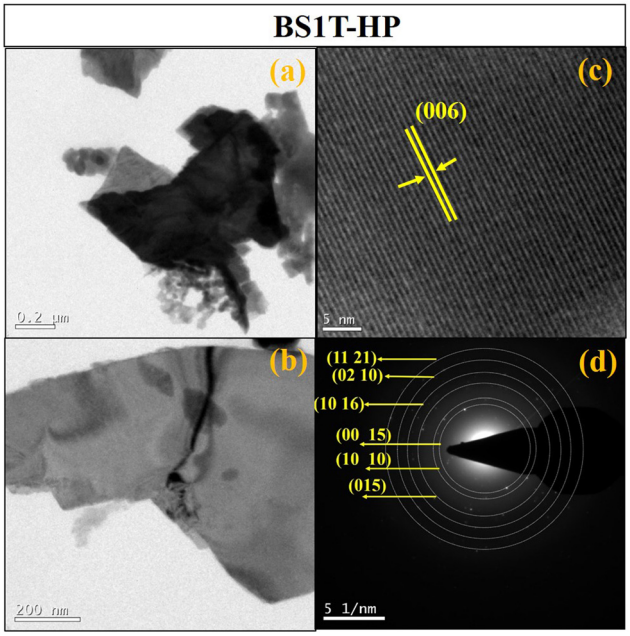

Fig. 6 (a) and (b) TEM images showing the formation of BS1T-HP nanosheets. (c) (006) plane corresponding to Bi_2Te_3 and (d) SAED patterns of BS1T-HP.

attachment occurs along a preferred direction, resulting in the formation of nanosheets. The (006) plane and the SAED patterns shown in Fig. 6(c) and (d) correspond to the lattice planes of Bi_2Te_3.

3.6. Mechanism for the formation of hot-pressed Sb-doped Bi_2Te_3

The detailed reaction mechanism showing the formation of Bi_2Te_3 nanostructures was reported in our earlier studies.[48] The mechanism for the formation of $Bi_{2-x}Sb_xTe_3$ nanostructures using EDTA is demonstrated in Fig. 7. Here, the secondary phases of Sb and Sb_2O_3 present in the as-prepared BS3T and BS5T disappear upon hot pressing. This could be due to the additional energy provided during hot pressing, which results in the phase formation of $Bi_{2-x}Sb_xTe_3$ nanostructures. The TEM images indicate the formation of sheet-like structures of BS1T-HP. It is well known that EDTA is a multidentate ligand with polyfunctional groups, and it could effectively serve as a bridging ligand to form multinuclear complexes with metal ions above some critical concentration. Then, chains of crystalline seeds would form in the nucleation process, especially with reaction time, which finally yields sheet/rod-like structures of the desired compound. The present approach using the reflux technique could favour the reaction mechanism through nucleation and growth processes. The crystalline $Bi_{2-x}Sb_xTe_3$ structures could form in the reflux reaction process through a homogeneous nucleation process if the reaction time is a varying parameter along with EDTA concentration. It is well known that the bismuth tellurium-based materials have a highly anisotropic structure, which favours the growth, primarily confined to a particular direction and the crystalline seeds of the material tend to grow into the rod/sheet shape under the influence of EDTA, which would be a soft template, and induce the formation of 1D/2D structures. Hence, EDTA could promote preferential directional growth under the template effect, where the formation of inorganic nanoparticles in liquid media is associated with monomer growth. Previous reports suggest that the nucleus is characterized by various shapes and facets with different surface energies and grows by bonding with other monomers in the solution. Crystal surface energy and facet attachment highly influence nanoparticle growth and shape formation. If any capping agent is present in the solution, it could bind to specific facets of the nucleus to coat it with a monolayer, which precisely occurs between Bi and EDTA in the present technique. These attached surfactants could lower the total surface energy when $Bi_{2-x}Sb_xTe_3$ nanocrystals are formed, specifically by blocking high-energy facets and exposing low-energy facets.

3.7. Seebeck coefficient, electrical resistivity and power factor of hot-pressed Sb-doped Bi_2Te_3

Fig. 8 shows the temperature dependence of S in the temperature range of 280–480 K. A negative value of S is obtained for BS1T at temperatures below 425 K, revealing an n-type semiconducting behaviour indicating that electrons are the majority carriers up to 425 K. As the temperature increases to 425 K, a clear transition from a negative to a positive value of S is evident, which marks a crossover from the n-type to the p-type. As the Sb doping concentration increases to 5%, the sample becomes completely p-type, which is evident from the obtained positive values of S from Fig. 8. Hence, an n-type to p-type semiconducting behaviour has been achieved with Sb doping in Bi_2Te_3. However, due to the presence of mixed phases in BS1T-HP, the value of S is quite low, reaching a maximum value of -54.78 μV K^{-1} at 306 K and 11.2 μV K^{-1} at 448 K. In the case of BS5T-HP, a maximum value of 215.12 μV K^{-1} is achieved at 465 K, which is remarkable.

To understand the electrical transport behaviour of the synthesized Sb-doped BT nanostructures, a detailed resistivity analysis was performed on the BS1T-HP and BS5T-HP samples in the temperature range of 280–480 K. Fig. 9 presents the temperature-dependent ρ of these samples, and reveals the semiconducting behaviour for BS1T-HP and BS5T-HP. BS1T-HP exhibits a ρ value of 0.00347 Ω m and BS5T-HP exhibits 0.01848 Ω m at 300 K, which is much higher than the values obtained for the BT samples reported recently.[48] Due to this, a considerable decrease in electrical conductivity can happen, which could ultimately lower the PF.

The temperature variation of PF, which is calculated as $S^2\sigma$, is plotted and shown in Fig. 10. The PF value of the BS1T-HP sample decreases with temperature, giving a maximum of 0.89 μW m^{-1} K^{-2} at 306 K and this low value of PF is arising due to the decreased S and increased ρ value compared to the Bi_2Te_3 samples discussed in the previous section. With the increase in Sb concentration in BS5T-HP, the PF follows an inverse trend where it increases with an increase in temperature, reaching a maximum value of 7.1 μW m^{-1} K^{-2} at 465 K. The decreased

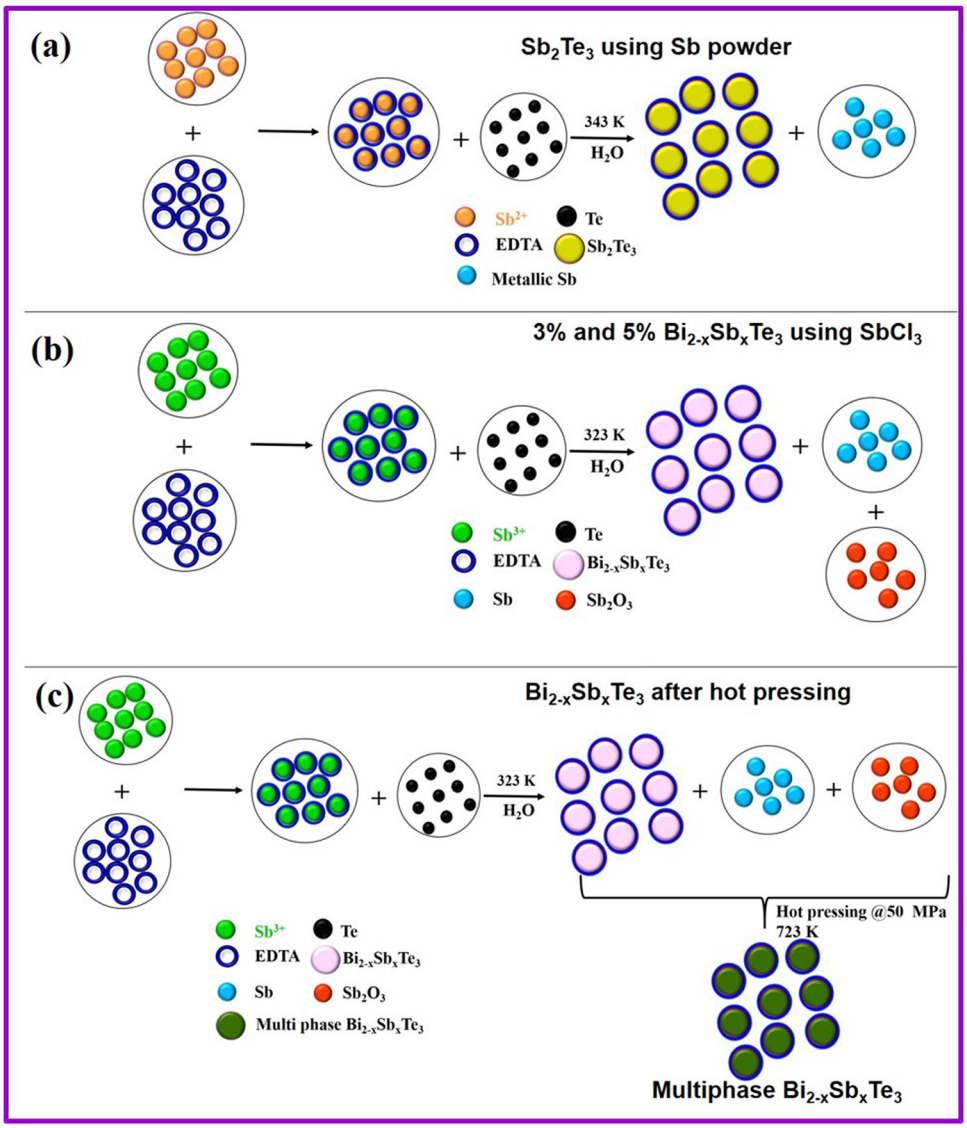

Fig. 7 Schematic showing the formation of EDTA-assisted (a) ST1, (b) 3% and 5% $Bi_{2-x}Sb_xTe_3$ and (c) hot-pressed $Bi_{2-x}Sb_xTe_3$ nanostructures.

value of PF in BS1T-HP could be attributed to the presence of multiphases of Bi_2Te_3 and BiTe present in the system. It could also be seen that there is a crossover from n-type (negative Seebeck) to p-type (positive Seebeck) in BS1T-HP at 440 K, as

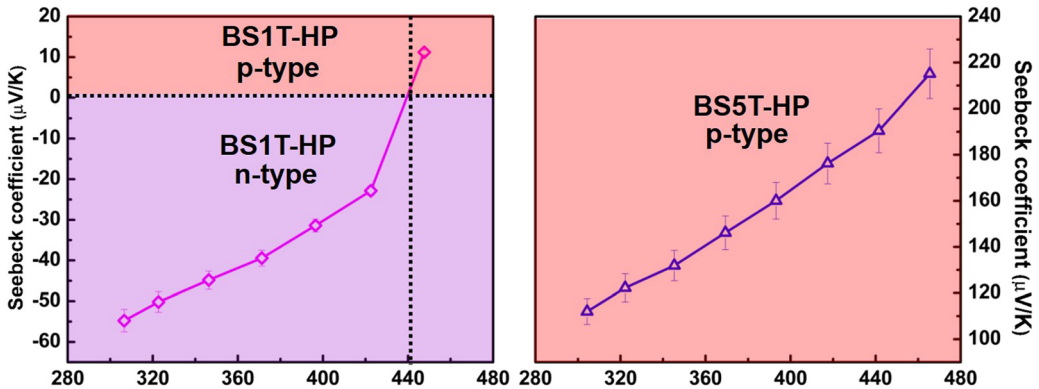

Fig. 8 Temperature dependence of Seebeck coefficient (S) of BS1T-HP and BS5T-HP samples.

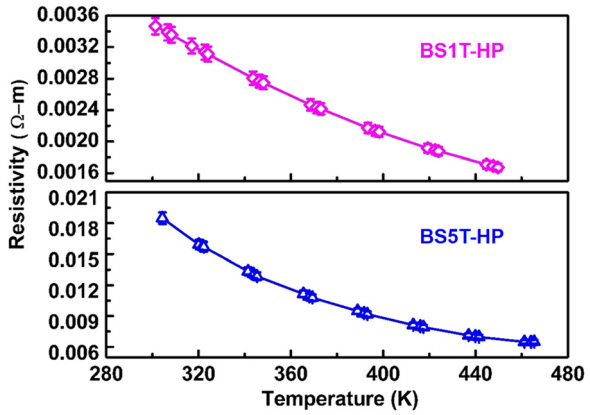

Fig. 9 Temperature dependence of resistivity (ρ) of BS1T-HP and BS5T-HP.

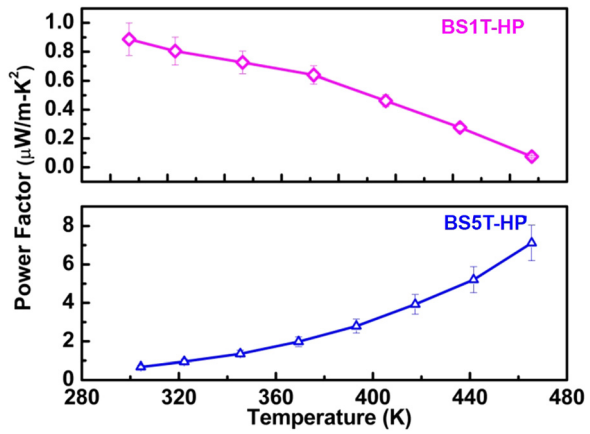

Fig. 10 Temperature dependence of PF of BS1T-HP and BS5T-HP.

shown in Fig. 8. For BS5T-HP, the material becomes completely p-type and Brahmi *et al.* reported that this transition could be due to the movement of the Fermi level (E_F) away from the conduction band and towards the valence band caused by the increased contribution from acceptors by changing the temperature.[50] This result could provide a new pathway towards finding the appropriate reaction mechanism and doping scheme for tailoring the TE properties for novel technological applications.

4. Conclusion

In summary, the Sb-doped Bi_2Te_3 nanostructures were synthesised successfully by a simple, low-cost and low-temperature reflux method using deionized water as the solvent. Structural and morphological changes were obtained by varying the reaction time in 75 mmol EDTA, which is confirmed by XRD and TEM analyses. The reaction mechanism for Bi_2Te_3, Sb_2Te_3 and SnTe was investigated in detail. Mechanism for the decomposition of EDTA and the concentration of which could facilitate the formation of chalcogenide nanostructures is explained. EDTA behaves not only as a capping agent but also as a soft template for lowering the surface energy, which could be the reason for the formation of sheet-like structures in Sb-doped Bi_2Te_3. An n-type semiconducting behaviour is witnessed for the 1% Sb-doped Bi_2Te_3 at temperatures below 440 K, and above this, a clear transition of semiconducting behaviour from the n-type to p-type is observed. Upon further increase in Sb concentration to 5%, the sample becomes completely p-type. Thus, it is understood that the hot-pressed Sb-doped Bi_2Te_3 shows an n-type to p-type semiconducting behaviour as a function of both temperature and Sb dopant concentration. However, the 5% Sb-doped Bi_2Te_3 exhibits a power factor value of 7.1 $\mu W\ m^{-1}\ K^{-2}$ at 465 K. These results indicate that Bi and Sb-based chalcogenide nanostructures could be synthesized successfully at low temperatures using a simple aqueous-based reflux technique, where appropriate reaction pathways could help in the formation of phase pure compounds, enhancing the overall thermoelectric performance of nanostructured chalcogenide materials.

Data availability

The data supporting this article have been included as part of the ESI.†

Conflicts of interest

The authors declare that they have no known competing financial interests or personal relationships that could have appeared to influence the work reported in this paper.

Acknowledgements

The authors would like to acknowledge the financial support received from the Council of Scientific and Industrial Research (CSIR), Govt. of India. V. R. A. is thankful to the Academy of Scientific and Innovative Research and CSIR for granting the Fellowship. The authors would also like to thank the Department of Science and Technology sponsored project number SPF/2023/00018 for partially supporting this work. M Vasundhara acknowledges the support offered by the Department of K&IM (IICT/Pubs./2024/117).

References

1 V. R. Akshay, M. V. Suneesh and M. Vasundhara, Tailoring Thermoelectric Properties through Structure and Morphology in Chemically Synthesised n-type Bismuth Telluride Nanostructures, *Inorg. Chem.*, 2017, **56**, 6264.
2 L. Yang, Z.-G. Chen, M. Hong, G. Han and J. Zou, *ACS Appl. Mater. Interfaces*, 2015, **7**, 23694–23699.
3 M. N. Touzelhaev, P. Zhou, R. Venkatasubramanian and K. B. Goodson, Thermal characterization of Bi_2Te_3/Sb_2Te_3 superlattices, *J. Appl. Phys.*, 2001, **90**, 763.
4 Y. Kim, A. DiVenere, G. K. L. Wong, J. B. Kelterson, S. Cho and S. J. R. Meyer, Structural and thermoelectric transport

properties of Sb_2Te_3 thin films grown by molecular beam epitaxy, *J. Appl. Phys.*, 2002, **91**, 715.
5 D. D. Frari, S. Diliberto, N. Stein and J. M. Lecuire, Comparative study of the electrochemical preparation of Bi_2Te_3, Sb_2Te_3, and $(Bi_xSb_{1-x})_2Te_3$ films, *Thin Solid Films*, 2005, **483**, 40.
6 S. Schulz, S. Heimann, J. Friedrich, M. Engenhorst, G. Schierning and W. Assenmacher, Synthesis of hexagonal Sb_2Te_3 nanoplates by thermal decomposition of the single-source precursor $(Et_2Sb)_2Te$, *Chem. Mater.*, 2012, **24**, 2228.
7 P. Dharmaiah, H. S. Kim, C. H. Lee and S. J. Hong, Influence of powder size on thermoelectric properties of p-type 25%Bi_2Te_3-75%Sb_2Te_3 alloys fabricated using gas-atomization and spark plasma sintering, *J. Alloys Compd.*, 2016, **686**, 1.
8 J. Horak, C. Drasar, R. Novotny, S. Karamazov and P. Lostak, Non-stoichiometry of the crystal lattice of antimony telluride, *Phys. Status Solidi A*, 1995, **149**, 549.
9 R. Venkatasubramanian, E. Siivola, T. Colpitts and B. O. Quinn, Thin-film thermoelectric devices with high room-temperature figures of merit, *Nature*, 2011, **413**, 597.
10 H. Q. Yang, L. Miao and C. Y. Liu, *et al.*, A facile surfactant-assisted reflux method for the synthesis of single-crystalline Sb_2Te_3 nanostructures with enhanced thermoelectric performance, *ACS Appl. Mater. Interfaces*, 2015, **7**, 14263.
11 J. Horak, Z. Stary and J. Klikorka, Relations between structure, bonding, and nature of point defects in layered crystals of tetradymite structure, *Phys. Status Solidi B*, 1988, **147**, 501.
12 W. Z. Wang, B. Poudel, J. Yang, D. Z. Wang and Z. F. Ren, High-yield synthesis of single-crystalline antimony telluride hexagonal nanoplates using a solvothermal approach, *J. Am. Chem. Soc.*, 2005, **127**, 13792.
13 M. Zhou, Z. M. Gibbs, H. Wang, Y. M. Han, C. N. Xin, L. F. Li and G. J. Snyder, Optimization of thermoelectric efficiency in SnTe: the case for the light band, *Phys. Chem. Chem. Phys.*, 2014, **16**, 20741.
14 J. He, J. T. Xu, G. Q. Liu, H. Z. Shao, X. J. Tan, Z. Liu, J. Xu, H. Jiang and J. Jiang, Enhanced thermopower in rock-salt SnTe–CdTe from band convergence, *RSC Adv.*, 2016, **6**, 32189.
15 X. J. Tan, H. Z. Shao, J. He, G. Q. Liu, J. T. Xu, J. Jiang and H. C. Jiang, Band engineering and improved thermoelectric performance in M-doped SnTe (M = Mg, Mn, Cd, and Hg), *Phys. Chem. Chem. Phys.*, 2016, **18**, 7141.
16 V. Vedeneev, S. Krivoruchko and E. Sabo, Tin Telluride Based Thermoelectrical Alloys, *Semiconductors*, 1998, **32**, 241.
17 R. F. Brebrick and A. J. Strauss, Anomalous Thermoelectric Power as Evidence for Two-Valence Bands in SnTe, *Phys. Rev.*, 1963, **131**, 104.
18 R. F. Brebrick, Deviations from stoichiometry and electrical properties in SnTe, *J. Phys. Chem. Solids*, 1963, **24**, 27.
19 L. M. Rogers, Br. Valence band structure of SnTe, *J. Appl. Phys.*, 1968, **1**, 845.
20 B. A. Efimova, V. I. Kaidanov, B. Y. Moizhes and I. A. Chernik, Band model of SnTe, *Phys. Solid State*, 1966, **7**, 2032.
21 W. Li, Y. Wu, S. Lin, Z. Chen, J. Li, X. Zhang, L. Zheng and Y. Pei, Advances in Environment-Friendly SnTeThermoelectrics, *ACS Energy Lett.*, 2017, **2**(10), 2349.
22 A. Banik, U. S. Shenoy, S. Anand, U. V. Waghmare and K. Biswas, Mg Alloying in SnTe Facilitates Valence Band Convergence and Optimizes Thermoelectric Properties, *Chem. Mater.*, 2015, **27**(2), 581.
23 A. Banik and K. Biswas, Lead-free thermoelectrics: promising thermoelectric performance in p-type $SnTe_{1-x}Se_x$ system, *J. Mater. Chem. A*, 2014, **2**, 9620.
24 M. K. Han, J. Androulakis, S. J. Kim and M. G. Kanatzidis, Lead-Free Thermoelectrics: High Figure of Merit in p-type AgSnmSbTem + 2, *Adv. Energy Mater.*, 2012, **2**, 157.
25 Y. Chen, M. D. Nielsen, Y.-B. Gao, T. J. Zhu, X. Zhao and J. P. Heremans, SnTe– $AgSbTe_2$ Thermoelectric Alloys, *Adv. Energy Mater.*, 2012, **2**, 58.
26 L. D. Zhao, H. J. Wu, S. Q. Hao, C. I. Wu, X. Y. Zhou, K. Biswas, J. Q. He, T. P. Hogan, C. Uher, C. Wolverton, V. P. Dravid and M. G. Kanatzidis, All-scale hierarchical thermoelectrics: MgTe in PbTe facilitates valence band convergence and suppresses bipolar thermal transport for high performance, *Energy Environ. Sci.*, 2013, **6**, 3346.
27 H. Wang, Z. M. Gibbs, Y. Takagiwa and G. J. Snyder, Tuning bands of PbSe for better thermoelectric efficiency, *Energy Environ. Sci.*, 2014, **7**, 804.
28 B. Gao, J. Tang, F. Meng and W. Li, Band manipulation for high thermoelectric performance in SnTe through heavy CdSe alloying, *J. Materiomics*, 2019, **5**(1), 111.
29 Q. Zhang, B. Liao, Y. Lan, K. Lukas, W. Liu, K. Esfarjani, C. Opeil, D. Broido, G. Chen and Z. Ren, High thermoelectric performance by resonant dopant indium in nanostructured SnTe, *Proc. Natl. Acad. Sci. U. S. A.*, 2013, **110**, 13261.
30 G. Tan, L. D. Zhao, F. Shi, J. W. Doak, S.-H. Lo, H. Sun, C. Wolverton, V. P. Dravid, C. Uher and M. G. Kanatzidis, High thermoelectric performance of p-type SnTe via a synergistic band engineering and nanostructuring approach, *J. Am. Chem. Soc.*, 2014, **136**, 7006.
31 G. Tan, F. Shi, J. W. Doak, H. Sun, L. D. Zhao, P. Wang, C. Uher, C. Wolverton, V. P. Dravid and M. G. Kanatzidis, Extraordinary role of Hg in enhancing the thermoelectric performance of p-type SnTe, *Energy Environ. Sci.*, 2015, **8**, 267.
32 U. Nithiyanantham, R. E. Sivasankara, M. Fevzi Ozaydin, H. Liang, A. Rathishkumar and S. Kundu, Low temperature, shape-selective formation of Sb_2Te_3 nanomaterials and their thermoelectric applications, *RSC Adv.*, 2015, **5**, 89621.
33 Y. D. Yin, Y. Lu, Y. G. Sun and Y. N. Xia, Silver nanowires can be directly coated with amorphous silica to generate well controlled coaxial nanocables of silver/silica, *Nano Lett.*, 2002, **2**, 427.
34 X. Peng, L. Manna and W. Yang, *et al.*, Shape control of CdSe nanocrystals, *Nature*, 2000, **404**(6773), 59.
35 L. Manna, E. C. Scher and A. P. Alivisatos, Synthesis of soluble and processable rod-, arrow-, teardrop-, and tetrapod-shaped CdSe nanocrystals, *J. Am. Chem. Soc.*, 2000, **122**(51), 12700.
36 Y. C. Ha, H. J. Sohn, G. J. Jeong, C. K. Lee and K. I. Rhee, Electrowinning of Tellurium from Alkaline Leach Liquor of Cemented Te, *J. Appl. Electrochem.*, 2000, **30**, 315.

37 R. S. Mane, B. R. Sankapal and C. D. Lokhande, Studies on Chemically Deposited Nanocrystalline Bi_2S_3 Thin Films, *Mater. Res. Bull.*, 2000, **35**, 587.

38 S. P. Summers, K. A. Abbound, S. R. Farrah and G. J. Palenik, Syntheses and Structures of Bismuth (III) Complexes with Nitrilotriacetic Acid, Ethylenediaminetetraacetic Acid, and Diethylenetriaminepentaacetic Acid, *Inorg. Chem.*, 1994, **33**, 88.

39 R. J. Mehta, Y. Zhang, C. Karthik, B. Singh, R. W. Siegel, T. Borca-Tasciuc and G. Ramanath, A new class of doped nanobulk high-figure-of-merit thermoelectrics by scalable bottom-up assembly, *Nat. Mater.*, 2012, **11**, 233.

40 J. S. Son, M. K. Choi, M.-K. Han, K. Park, J.-Y. Kim, S. J. Lim, M. Oh, Y. Kuk, C. Park, S.-J. Kim and T. Hyeon, n-Type Nanostructured thermoelectric materials prepared from chemically synthesized ultrathin Bi_2Te_3 nanoplates, *Nano Lett.*, 2012, **12**, 640.

41 P. Kumar, P. Srivastava, J. Singh, R. Belwal, M. K. Pandey, K. S. Hui, K. N. Hui and K. Singh, Morphological Evolution and Structural Characterization of Bismuth Telluride (Bi2Te3) Nanostructures, *J. Phys. D: Appl. Phys*, 2013, **46**, 285301.

42 A. E. Martell, R. J. Motekaitis, A. R. Fried, J. S. Wilson and D. T. Macmillian, Thermal decomposition of EDTA, NTA and Nitrilotrimethylenephosphonic acid in aqueous solution, *Can. J. Chem.*, 1975, **53**, 3471.

43 Y. Deng, C.-W. Nan and L. Guo, A novel approach to Bi_2Te_3 nanorods by controlling oriented attachment, *Chem. Phys. Lett.*, 2004, **383**, 572.

44 S. Gupta, S. Neeleshwar, V. Kumar and Y. Y. Chen, Synthesis of bismuth telluride nanostructures by refluxing method, *Adv. Mater. Lett.*, 2012, **3**(1), 50.

45 H. Q. Yang, L. Miao, C. Y. Liu, C. Li, S. Honda, Y. Iwamoto, R. Huang and S. Tanemura, A Facile Surfactant-Assisted Reflux Method for the Synthesis of. Single-Crystalline Sb_2Te_3 Nanostructures with Enhanced Thermoelectric Performance, *ACS Appl. Mater. Interfaces*, 2015, **7**(26), 14263.

46 P. Dharmaiah and S.-J. Hong, Hydrothermal method for the synthesis of Sb_2Te_3 and $Bi_{0.5}Sb_{1.5}Te_3$ nanoplates and their thermoelectric properties, *Int. J. Appl. Ceram. Technol.*, 2017, **15**(1), 132.

47 H. Kodama, S. Horiuchi and A. Watanabe, The hydrothermal synthesis of bismuth oxide chlorides, *J. Solid State Chem.*, 1988, **75**, 279.

48 V. R. Akshay, B. Arun, M. V. Suneesh and M. Vasundhara, Surfactant Induced Structural Phase Transitions and Enhanced Room Temperature Thermoelectric Performance in n-Type Bi_2Te_3 Nanostructures Synthesized via Chemical Route, ACS Applies, *Nanomaterials*, 2018, **1**(7), 3286.

49 G. Han, R. Zhang, S. R. Popuri, H. F. Greer, M. J. Reece, J.-W. G. Bos, W. Zhou, A. R. Knox and D. H. Gregory, Large-Scale Surfactant-Free Synthesis of p-Type SnTe Nanoparticles for Thermoelectric Applications, *Materials*, 2017, **10**, 233.

50 H. Brahmi, R. Neupane, L. Xie, S. Singh, M. Yarali, G. Katwal, S. Chen, M. Paulose, O. K. Varghese and A. Mavrokefalos, Observation of a low temperature n–p transition in individual titania nanotubes, *Nanoscale*, 2018, **10**, 3863.